Medical Engineering & Physics 34 (2012) 929–937

Contents lists available at SciVerse ScienceDirect

Medical Engineering & Physics

journal homepage: www.elsevier.com/locate/medengphy

Three-Dimensional Printing (3DP) of neonatal head phantom for ultrasound: Thermocouple embedding and simulation of bone

Matteo Gatto[a,*], Gianluca Memoli[b], Adam Shaw[b], Neelaksh Sadhoo[b], Pierre Gelat[b], Russell A. Harris[a]

[a] Wolfson School of Mechanical and Manufacturing Engineering, Loughborough University, LE11 3TU, United Kingdom
[b] Acoustics and Ionising Radiation Division, National Physical Laboratory, Teddington, United Kingdom

ARTICLE INFO

Article history:
Received 14 April 2011
Received in revised form 6 October 2011
Accepted 24 October 2011

Keywords:
Three-Dimensional Printing
Rapid Prototyping
Ultrasound
Phantom
Embedding
Thermocouple
Rapid Tooling

ABSTRACT

A neonatal head phantom, comprising of an ellipsoidal geometry and including a circular aperture for simulating the fontanel was designed and fabricated, in order to allow an objective assessment of thermal rise in tissues during trans-cranial ultrasonic scanning of pre-term neonates. The precise position of a series of thermocouples was determined on the basis of finite-element analysis, which identified crucial target points for the thermal monitoring within the phantom geometry. Three-Dimensional Printing (3DP) was employed for the manufacture of the skull phantom, which was subsequently filled with dedicated brain-mimic material. A novel 3DP material combination was found to be able to mimic the acoustic properties of neonatal skull bone. Similarly, variations of a standard recipe for tissue mimic were examined, until one was found to mimic the brain of an infant. A specific strategy was successfully pursued to embed a thermocouple within the 3DP skull phantom during the manufacturing process. An in-process machine vision system was used to assess the correct position of the deposited thermocouple inside the fabricated skull phantom. An external silicone-made skin-like covering completed the phantom and was manufactured through a Direct Rapid Tooling (DRT) technique.

1. Introduction

Ultrasound technologies are broadly employed for imaging and diagnostic purposes in medical applications involving soft tissue structures. In addition to the widely known intrauterine foetal imaging, there are other cases where ultrasonography is considered an essential, non-invasive, imaging tool. A key example is trans-cranial imaging, commonly used to diagnose congenital and acquired anomalies of the neonatal brain, particularly in premature babies and in the first weeks after birth [1]. As reported in many manuals [2] sonography of the neonatal brain is generally carried out through the anterior fontanel. The fontanels (or fontanelles) are two anatomical, diamond-shaped apertures in the skull of neonates which normally ossifies between the 7th and 19th month. Nevertheless, the effects of prolonged exposure to a high ultrasonic field (i.e. a high "ultrasonic dose") and the consequent risks for the target tissues have not been documented by epidemiological studies.

Ultrasound scanning, however, is known to cause heating in biological tissue [3]. This aspect may be particularly relevant since trainees or less experienced clinicians, in this particular case, may require more time to detect target brain structures. While there are specific guidelines for building validated phantoms to measure the exposure to ionising radiations [4] – including prescriptions for skull, brain, skin, liquid within the skull – nothing so detailed exists for ultrasound. A study with a dedicated phantom is therefore appropriate.

This study was part of a larger project established at the NPL and the Royal United Hospital of Bath (RUH) and funded by the UK Department of Health (DH), which aimed at investigating the safe use of ultrasound for neonatal head scanning. The project proposed to design a validated, clinically relevant phantom to be used in a hospital survey across the UK. The scope was to measure the temperature increase caused by ultrasound equipment currently used in neonatal head scanning, using a repeatable and traceable protocol [5].

A realistic ultrasound phantom, mimicking the morphological and acoustic properties of neonatal skull tissue and able to measure the temperature variations during ultrasound examination, could be employed as ultrasound training tool. Current phantoms employed in ultrasonography are relatively simplistic and they only allow practising of rudimentary skills. Areas of interests, such as vessels or pathological masses are reproduced with basic geometries, conventionally cylinders, spheres or disks [6,7]. In addition, they do not include any specific component (e.g. thermocouple) for the temperature measurement, not only for technical reasons, but

* Corresponding author. Tel.: +44 (0) 1509 227571.
E-mail addresses: gatto_matteo@libero.it (M. Gatto), gianluca.memoli@npl.co.uk (G. Memoli), adam.shaw@npl.co.uk (A. Shaw), neelaksh.sadhoo@npl.co.uk (N. Sadhoo), pierre.gelat@npl.co.uk (P. Gelat), r.a.harris@lboro.ac.uk (R.A. Harris).

1350-4533/$ – see front matter © 2011 IPEM. Published by Elsevier Ltd. All rights reserved.
doi:10.1016/j.medengphy.2011.10.012

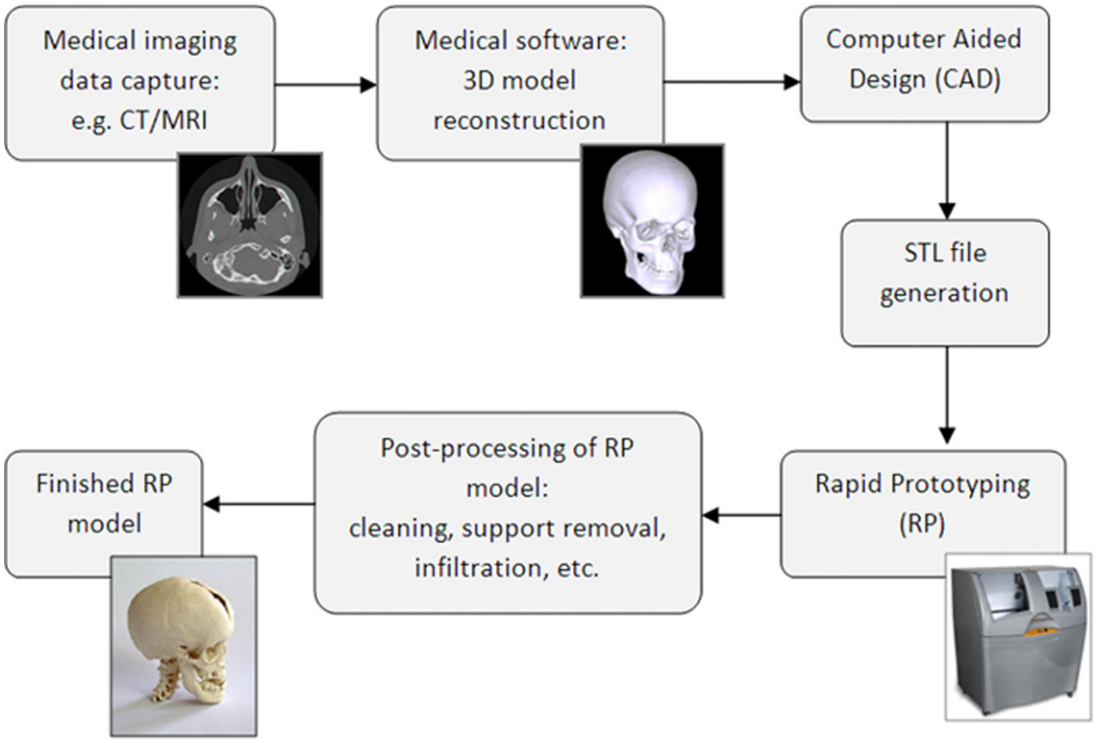

Fig. 1. Sequence of steps followed during the Rapid Prototyping (RP) of a medical model.

also as a possible training tool. An anatomically relevant phantom would allow images to be produced at leisure, without exposure of real neonates.

Some works pioneered the adoption of Rapid Prototyping (RP) technology for the manufacturing of simulation phantoms for ultrasound testing [8,9]. These Additive Manufacturing (AM) approaches enable the reproduction of complex structures which could not be manufactured with conventional techniques (e.g. moulding, investment casting, milling, etc.). A typical procedure to produce RP models for medical applications can be seen in Fig. 1. In this research, Three-Dimensional Printing (3DP) technology by ZCorporation® (Burlington, USA), appeared the most appropriate for the manufacturing of bone-simulation materials. In 3DP, a thin layer of plaster powder is spread on a powder bed. Then, an inkjet head moves in the *xy* plane, jetting a liquid binder over the powder bed, allowing the binding of powder particles. Once the first cross-sectional layer of the part is completed, the piston is lowered by approximately 0.1 mm and a new layer of powder is spread. The next layer is selectively jetted by the printheads. This cyclic process proceeds till completion of the part.

The porous structure of the green (untreated) 3DP part enables post-processing treatments, such as infiltration with secondary materials in a liquid format to allow a wide range of resulting physical properties to be achieved [10,11]. The ceramic nature of the primary build material (in this case ZP130™/ZB58™) could also be an advantage to replicate bone tissue characteristics [12]. The flexibility of 3DP and the variety of properties achievable through post-processing support the suitability of this process for ultrasound phantom manufacturing.

In order to replicate the acoustic properties of neonatal skull bone the correct infiltrant combination for the 3DP material had to be addressed. Several studies have analysed the ultrasonic properties of human bone [13,14] and others have looked at specific materials to mimic it. Materials such as glass-filled PTFE [15,16], epoxy materials [17,18], ebonite, fibreglass, carbon fibre plastics and acrylic [19] were all shown to approximate quite well with the acoustic properties of cortical bone. High density polyethylene, in particular, has been recommended as a foetal bone mimic [20] and, more recently, cortical bone substitutes have been made using epoxy resin, polymers and polymer composites [20]. Once the appropriate infiltrant was identified, it was then applied to the 3D printed skull phantom.

This paper reports the research conducted on the technical aspects of the design and fabrication of a neonatal skull phantom and its initial validation, through the feedback of the clinicians and comparison with theoretical modelling. The final results of the hospital survey and the research on the brain mimic will be discussed in another work.

2. Materials and methods

This investigation comprised of three main parts. The first consisted in the selection of a suitable 3DP material combination, able to replicate ultrasound properties of neonatal skull bone. The second part of the study concerned the manufacturing of a neonatal skull phantom with an embedded Fine-Wired Thermocouples (FWTC), which allowed the measurement of the thermal effects of ultrasound equipment on proximal tissues during the scanning. The last part focused on the design and fabrication of a silicone skin for the neonatal skull phantom using Rapid Tooling (RT) techniques.

2.1. Neonatal skull phantom specifications

2.1.1. Phantom geometry

In order to represent the anatomy of the typical neonatal head, both the dimensions of the head and those of the fontanel need to be known.

While average neonatal head sizes are well known and used to estimate the child's [21] health, the shape of the fontanel is more complex. Having excluded reverse engineering from CT data for its ethical implications, a suitable geometry of the neonatal skull

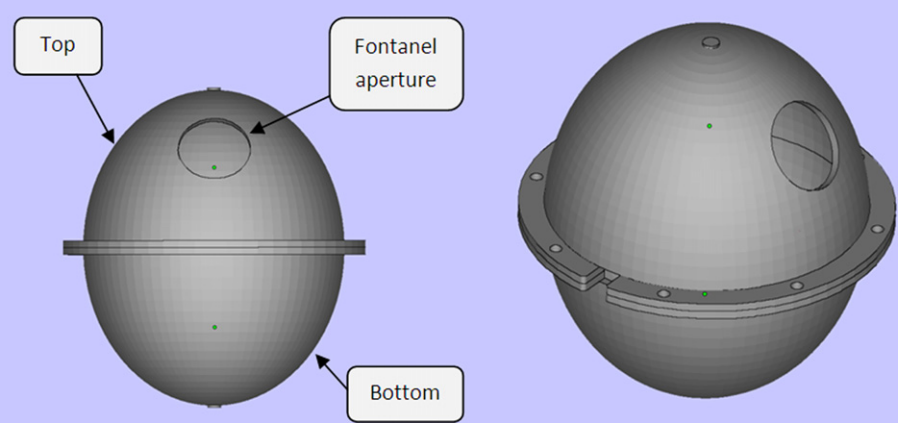

Fig. 2. STL file of the neonatal skull phantom used for ultrasound testing, which was to be fabricated with 3DP process. It comprises of two main elements (top and bottom). The fontanel has also been included in the geometry, while the equatorial notch allowed the two halves to be joint/separated when necessary.

phantom was produced (Fig. 2). Clinical requirements dictated that the phantom described in this study should:

- replicate the skull of a 28 weeks neonate (i.e. a pre-term baby);
- comprise a prolate ellipsoid (i.e. the skull) filled with brain-mimic material and covered with a simulated skin covering (1.5 mm thick);
- include a circular hole, with the same area and position of a typical fontanel at 28 weeks.

The dimensions of the oblate ellipsoid (Biparietal diameter: 75 mm, Occipito-frontal diameter: 92 mm) were obtained by intersecting the reference data commonly used in the neonatal units in the UK [21] with those reported in ICRP 2002. The dimensions of the fontanel were obtained from a recent study [22] that used 3D ultrasound imaging to look at fontanel size as a function of gestational age. His results indicate a typical diameter of 2.4 cm for ages above 24 weeks.

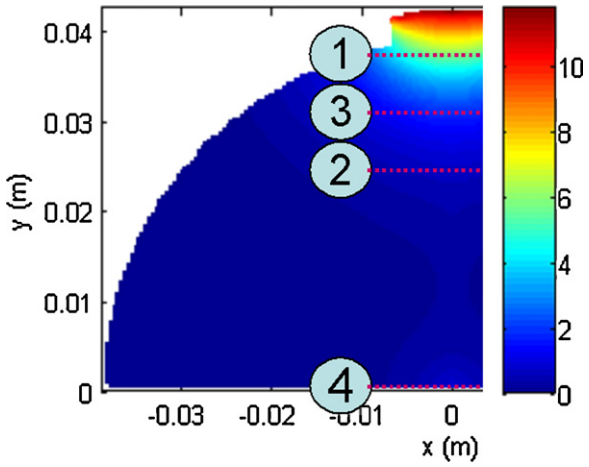

Fig. 3. Ideal position of the thermocouples according to FEM analysis performed by NPL investigators.

2.1.2. Target points for thermal monitoring within the phantom

Once the geometry was decided, it was necessary to identify the most important places where to monitor the temperature rise during ultrasound exposure. A quadrant containing regions of brain-like, tissue-like and bone-like media was then generated for the purpose of the vibroacoustic analysis. Finite element modelling using PAFEC and preliminary results with an initial design first version of phantom [5] permitted to calculate the temperature distribution (Fig. 3) in the case of a semi-spherical skull filled with brain-mimic material and subjected to the emission of a focussed cylindrical symmetric transducer through a hole in the skull (the fontanel). As a consequence of the modelling results, four important positions were selected for monitoring: (1) just below the transducer, under the skin-mimic; (2) in the bulk of the brain (3) between the skin and the bulk, to monitor the gradient; (4) in the bone opposite the fontanel, where the exciting transducer is.

Consequently, the phantom was to incorporate at least four thermocouples (TCs), one of which would be embedded in the portion of 3DP model of skull opposite the fontanel (TC No. 4), in order to effectively measure the thermal variation of the neonatal skull bone. The method of embedding the thermocouple is described in Section 2.3. Thermocouple No. 1 was to be attached between the skin and the fontanel, while the other two needed to be inserted within the brain.

2.2. Simulation of neonatal bone acoustic properties with 3DP materials

2.2.1. Manufacturing of 3DP test samples

A series of disks were 3D-printed – with a diameter of 50 mm and thicknesses of 2 mm, 3 mm and 5 mm – for measuring the acoustic properties of the 3DP material. A Z510™ Spectrum 3D printer was employed for the fabrication of the test samples. The 3DP parameters were set to the default values of the powder-binder combination of ZP130™ and ZB58™. The disk samples were oriented along the *xy* plane of the building chamber. Afterwards, the printed parts were extracted from the build chamber and accurately depowdered by air-blowing. Then, they were placed in an air-circulating oven at 80 °C for 2 h, and 120 °C for 1 h. This ensured the full curing of water-based binder within the parts and elimination of moisture which could impede infiltration.

The post-processing phase comprised of infiltrating the 3DP parts with liquid substances of: Clear Coat™ epoxy resin (System Three Resins Inc., Auburn, USA), Crystic® 2-414PA polyester resin (Scott Bader Ltd., Wellingborough, UK) and Paraplast™ X-TRA paraffin wax (McCormick Scientific™, Richmond, USA). Except for paraffin wax, the infiltration was performed by immersion, under vacuum conditions in a dedicated chamber. The samples were maintained at −95 kPa for 5 min, at a temperature of 25 °C. This period was limited by the cure-time of the infiltrant compounds

after which their viscosity was inevitably affected and, as a consequence, their penetration. Then, the atmospheric inlet valve was opened to relieve the vacuum, causing a further penetration of the infiltrant by atmospheric pressure action. Afterwards, the specimens were extracted from the chamber and the excess resin was wiped off the surface. Differently, paraffin wax was pre-heated to 70 °C in a specific oven, specifically developed for wax infiltration, and for this reason vacuum could not be applied. The samples were then introduced into the melted paraffin wax, and kept there for 10 min. The parts were extracted and cleaned of excess wax. All the infiltrated specimens were left for 72 h at 25 °C.

2.2.2. Measurement of the ultrasonic properties

The acoustical properties (speed and attenuation of sound) of the three candidate skull mimics were determined at the National Physical Laboratory using an insertion loss method with disk samples of approximately 2, 3 and 5 mm thickness. For each material, the three 3DP disks were acoustically characterised in the range 2–20 MHz and the values of the acoustical properties were obtained by interpolation. For each thickness, the transmission loss (in dB) could be obtained by fitting the data with a power law.

$$\text{Transmission loss (dB)} = \alpha_n \cdot f^{Bn}$$

with $n = 2, 3, 5$ to indicate the respective thickness (in mm).

If the material is the same, however, the dependency on frequency should be the same and differences among the fitting coefficients should be negligible (i.e. $B = B_2 = B_3 = B_5$). A least-square fit was therefore performed on all the data, constraining the exponent to be the same for the three thicknesses (i.e. with $\alpha_2, \alpha_3, \alpha_5, B$ as parameters).

Assuming that the coefficients α_n were only (linearly) dependent on thickness, the three results for α_n (one for each thickness, with a common exponent), were then used to find the attenuation coefficient of a fixed material, in dB cm^{-1}, with a reduced overall uncertainty. The frequency of 1 MHz was then selected as a reference for comparison with literature data (and therefore choose the optimal material to mimic the neonatal skull), which reported attenuation coefficients in dB cm^{-1}, as a non-linear function of frequency [28,29]. The reference frequency was chosen at 1 MHz as only near that value it was possible to find data for all the different parts of the neonatal skull (i.e. bone, brain, skin). In addition to this, at the frequency of 1 MHz, the attenuation coefficient of a selected material can be compared with values in dB cm^{-1} MHz^{-1} without ambiguity.

A similar process was applied to speed of sound measurements, which showed an almost flat dependence on frequency.

2.2.3. Depth of penetration (DOP) assessment

An additional series of cubic samples of 15 mm per side was also produced consistently with the method followed in Section 2.2.1, which were used for assessing the depth of penetration (DOP) of the applied infiltrant within the 3DP porous structure. Following curing, the test samples were sectioned along the middle vertical plane, in order to analyse the cross-section under a Smartscope® Flash™ 200 (OGP®, Rochester, USA) optical measuring apparatus. A red powdery pigment, traditionally used for resin colouring, was added to the infiltrant agents, in order to better identify the boundaries of infiltration. The DOP was measured in terms of distance from the edge of the sample to the edge of the coloured infiltrant, neglecting any excess layer of infiltrant material on the sample surface. The average DOP was calculated for each material combination.

2.3. Embedding of fine-wired thermocouples into the 3DP neonatal skull phantom

The neonatal skull phantom described in Section 2.1.1 (Fig. 2) was manufactured by 3DP process, following the same methodology described in Section 2.2.1.

A thermocouple (TC) was embedded into each of the two semi-spheres (position No 4 in Fig. 3) constituting the skull phantom, which were manufactured by 3DP process. The embedding of the TC specifically during the printing process was dictated by several factors. First, the poor accessibility of the skull phantom could be an obstacle to the positioning of the TC once the skull has been manufactured. More importantly, the in-process embedding would avoid the use of secondary materials, such as adhesives, that would hinder the response rate of the TC, and, consequently, affect the accuracy of the measurements. In addition, embedding ensured that the precise location of the thermocouple could be guaranteed.

A novel method was developed that allowed embedding during the 3DP build process. Although there was a wide range of alternative thermocouple types, only a few of these could be adopted. Following some preliminary tests, Fine-Wired Thermocouples (FWTCs) appeared the most suitable for this purpose. In this case, 0.005 in. (0.125 mm) FWTCs (Omega®, Manchester, UK) were selected. The sensitive junction of the FWTC had to be positioned at the top of the semi-sphere, as close as possible to the inner surface; in this case at approximately 0.5 mm from the inner surface (Fig. 4).

The in-process embedding of the TC comprised of several phases. After the 3DP job was started, the printer was paused at the specified layer. At this point, a new layer of unbound powder was present over the printed part, ready to be selectively bound by the jetted binder. The FWTC probe was then manually positioned on

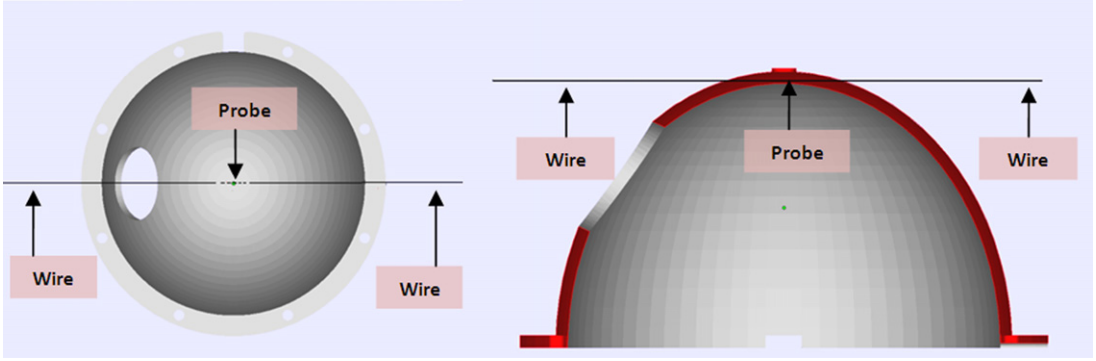

Fig. 4. Position and orientation of the embedded FWTC inside the 3DP neonatal skull phantom. The probe of the FWTC was centered at the top of the semi-sphere (left), allowing the two wires to exit from the two opposite sides. The sensitive junction (probe) of the FWTC had to be positioned at approximately 0.5 mm from the inner surface of the skull phantom, as shown on the section view of the semi-sphere (right).

Table 1
Components for the standard mix for the tissue-mimicking material in IEC 60601-2-37.

Component	Weight %
Water	82.95
Glycerol	11.21
Agar	3.02
Aluminium oxide (3 μm)	0.94
Aluminium oxide (0.3 μm)	0.88
Silicon carbide (400 mesh)	0.53
Benzalkonium chloride	0.47

the powder bed surface, along the *x*-axis of the printer to minimize the disruption caused by the roller during the spreading phase. The loose powder, surrounding the printed object, acted as a support and avoided possible displacements of the newly printed feature when depositing the FWTC. Once the FWTC was in place, the printing job was resumed, and the print-heads jetted the next layer of the built part. As the build progressed layer-by-layer, the FWTC was progressively embedded into the printed skull phantom.

The position of the deposited FWTC was monitored through the in-process video analysis to ensure accuracy and recording of the positioning prior and during the 3DP process steps. It was necessary to assess the location of the TC's probe inside the printed phantom, avoiding destructive methods, which would have been counterproductive. A dedicated machine vision apparatus [23] for Non-Destructive Analysis (NDA) of 3DP parts was employed for the in-process monitoring of the FWTC embedding. Alternatively, other non-destructive methods of analysis, such as ultrasound and micro-computed tomography (micro-CT), could have been employed, but they would not allow the identification and rectification of errors during production. The video system improved and verified the accuracy in placing the thermocouple on the powder bed. In addition, the acquired images of the built layers were analysed to calculate the position of the FWTC inside the phantom. Eventual displacement or rupture of the FWTC could be ascertained by this method.

2.4. Brain mimic for the neonatal skull phantom

The brain mimic material was based on a standard tissue-mimicking gel [24] as reported in Table 1. For this application, however, the attenuation coefficient of the standard gel is too high at approximately 0.5 dB cm^{-1} (at 1 MHz): results in the literature [25,26], give an attenuation coefficient of 0.16–0.3 dB cm^{-1} (at 1 MHz). A number of variations on the basic recipe have been therefore tested, in order to find the optimal material (in terms of value and frequency dependence, as previously described for the bone). Eventually, it was found that varying the content of Aluminium oxide was sufficient to achieve the desired result.

2.5. Skin covering for the neonatal skull phantom

An external skin-like covering was required to improve the realistic appearance of the neonatal skull phantom and aid the training purpose with regards accurate positioning at the fontanel. It is important to replicate the feel of skin in order to resemble a more realistic scenario. For this purpose, the skin had to be between 1.5 and 2.0 mm thick, and manufactured from a skin-simulating material, such as silicon rubbers, which have been used in the past to mimic skin, even if their properties slightly differ from the ones of skin and soft tissue [27]. A casting/moulding method was believed the most suitable for the skin production. In industrial applications, vacuum casting is largely adopted for the production of small series of parts. Some works have explored the use of RP technologies for direct mould or tool manufacturing, known as Direct Rapid Tooling (DRT) [28,29]. The RP mould can then be used for the casting process. The advantage of DRT is the ability to directly design the mould and produce part in a shorter time, by avoiding the manufacture of the master.

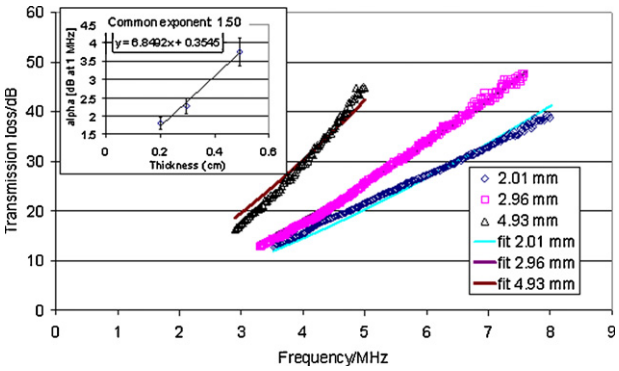

Fig. 5. Results of sound attenuation for the three disks of epoxy-infiltrated ceramic in the range 2–20 MHz. The inset shows the three values of attenuation in dB/MHz, extrapolated at 1 MHz, and the linear fit used to obtain a value not dependent on thickness.

The stereolithography (SLA) process was preferred to 3DP process for the final mould manufacturing. The single cross-sections of a model are obtained by the selective curing of a UV-curable photopolymer through a UV-laser. Specifically, a Viper® SLA (3DSystem®, Rock Hill, USA) available at Loughborough University was employed. The SLA machine used Accura® PEAK™ Plastic as the building material, which offered mechanical properties and appearance (i.e. clear) similar to polycarbonate. A suitable silicone material was identified for the casting. RTV2403 silicone (Techsil®, Bidford on Avon, UK) appeared the most promising for this purpose. It presented a relatively low viscosity (9000 MPa/s) and a slow curing rate, which were essential for the efficient filling of the narrow mould cavity. The skin covering had a thickness of 1.5 mm. The mould was designed using Magics software (Materialise, Leuven, Belgium), including inlet and vents.

3. Results

3.1.1. Acoustic properties of 3DP materials

Fig. 5 reports the measured values of transmission loss for three disks of epoxy-infiltrated ceramic (thickness 2, 3, 5 mm) as a function of frequency, in the range 3–8 MHz. The plots also report the fitting power laws: each with a different coefficient (α_2, α_3, α_5), but with the same exponent ($B = 1.50$ in this case). The inset in Fig. 5 shows how the three values of the attenuation (once extrapolated at 1 MHz) were used to obtain the final value of 6.85 ± 0.7 dB cm^{-1} (at 1 MHz) for epoxy infiltrated 3DP ceramic. The results of the overall analysis on attenuation have been summarised graphically in Fig. 6. Uncertainties on the coefficients were estimated to be of the order of 10%. The existing data from the literature [25,26] for skull bone in neonates have been reported in Table 2, together with the values from the analysis described in Section 2.2.2. As mentioned before, the values have been compared at the reference frequency of 1 MHz.

The resulting comparison with the target value (Table 2) identified that the ceramic infiltrated with epoxy resin, with an attenuation coefficient of 6.85 ± 0.7 dB cm^{-1} (at 1 MHz), was the best candidate to mimic neonatal cranial bone. The polyester resin samples, with an attenuation coefficient of 64.9 ± 6 dB cm^{-1} (at 1 MHz), presented acoustic properties in the range of adult skull bone, which has a higher attenuation coefficient than neonatal skull bone. A further drawback for the use of polyester resin was

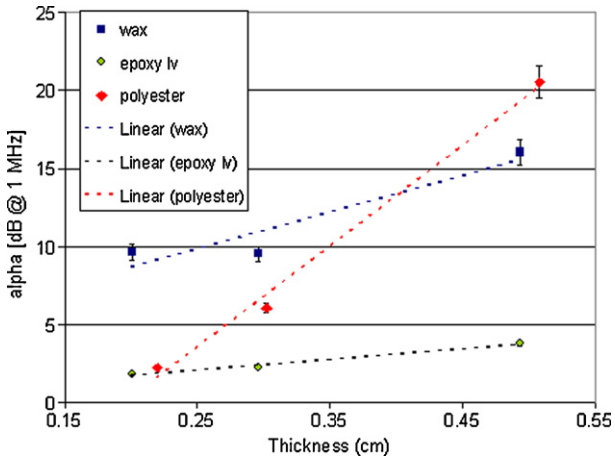

Fig. 6. Dependence of the attenuation coefficients on thickness of the disk samples of 3DP infiltrated materials.

represented by its considerable shrinkage (8%) which caused some distortion phenomena after the resin cured, which affected thin disk specimens of 2 and 3 mm thickness. Paraffin wax presented inconsistent transmission absorption values across the three different thicknesses, which could be due to some air bubbles trapped in the 3DP material during infiltration (which for wax was not completed under vacuum).

The DOP analysis showed that epoxy resin and polyester resin penetrated an average distance of 4.53 mm and 3.63 mm respectively, while paraffin wax was able to fully penetrate within the 3DP cubic specimen. The measured levels of penetration were adequate for infiltrating the features of the neonatal skull phantom of 2 mm thickness.

Finally, epoxy resin was identified as the appropriate 3DP infiltrant for the simulation of the acoustic properties of neonatal skull bone.

3.1.2. TC embedding

The images acquired during the phantom manufacturing and thermocouple embedding, permitted direct control over the entire procedure. It was interesting to see how the thermocouple was progressively embedded into the manufactured skull phantom after a few layers.

Measurements performed on the layer images assessed the location of each thermocouple probe (Table 3). The thermocouples were successfully embedded into the 3DP phantoms and positioned within the designated target area of 2 mm Ø in the xy building plane (Fig. 7). This novel method employed for the thermocouple embedding into 3DP part was successful. The roller movement during the powder spreading did not disturb or disrupt the thermocouple, as confirmed by the images acquired by the Non-Destructive Analysis (NDA) system.

Table 2
Comparison between the target values [25,26] and the candidate materials for skull bone. Values have an uncertainty of 10%.

Infiltrant	Attenuation coefficient [$dB^{-1}\,cm^{-1}$] (at 1 MHz)	Power dependence of attenuation with frequency	
		Coefficient α [$dB^{-1}\,cm^{-1}\,MHz^{-k}$]	Exponent k
Epoxy	6.85	6.85	1.50
Polyester	64.9	64.9	1.37
Wax	23.6	23.6	0.97
Target value	5–7 for neonates	5–7 for neonates	1.2–2.1

Table 3
Results from FWTC position measurements by imaging analysis (±0.03 mm). The target position has been set as origin of the coordinate system.

3DP part	X (mm)	Y (mm)	Distance (mm)
Back-1	0.39	0.09	0.40
Back-2	0.10	0.60	0.60
Front-1	0.90	0.30	0.96
Front-2	0.27	0.03	0.27

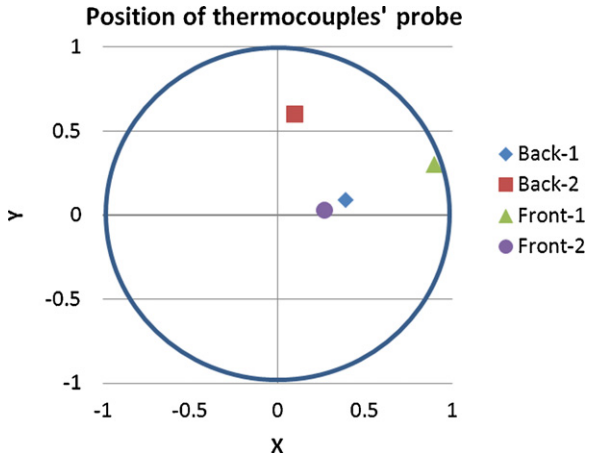

Fig. 7. Plot of positions of thermocouples' probes within the target area of 2 mm diameter calculated with the video system. All the probes were correctly positioned within the specified area.

3.1.3. Results of brain mimic material

As mentioned before, a number of variations on the basic recipe [24] have been tested and it has been found that changing the concentration of aluminium oxide could vary the attenuation coefficient and its dependence on frequency. The attenuation coefficient and speed of sound were measured as a function of frequency using the materials characterisation facility at NPL (previously used for the bone mimic) for different concentrations. At 50% of the standard concentration (0.91 g/l), in fact, the attenuation and speed of sound in the gel fell within the range of target values (Table 4): this material was chosen as brain mimic.

3.1.4. Results of skin fabrication

The Viper SLA provided a rigid mould with excellent cosmetic properties. The building time was around 18 h. After manufacturing, the mould was placed into a UV oven for 24 h, to allow complete curing of the resin. The STL facets were still visible on the curved surface of the mould after cure, therefore sanding was performed manually with 320 grit and 600 grit sandpaper in order to smooth

Table 4
Summary of acoustic properties of 3 variations of brain mimic compared to target values. Speed of sound values have an uncertainty of 0.5%, attenuation coefficients of 10%.

Conc. of Al_2O_3 (g/l)	Speed of sound (m/s)	Attenuation coefficient [$dB\,cm^{-1}$] (at 1 MHz)
0.91	1528	0.264
1.82	1531	0.437
2.73	1537	0.571
Target value	1528 at 28 weeks; increasing with age	0.16–0.3

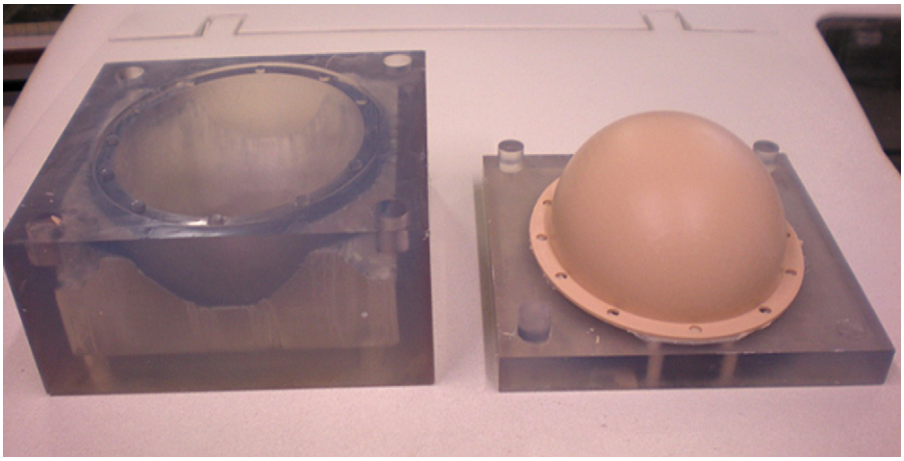

Fig. 8. SLA rigid mould produced with Viper™ SLA machine. The mould was successful for the casting of the skin covering, produced with a low-viscosity silicone (right).

the mould surface. Prior to the casting process a release agent was sprayed over the mould's surface to avoid the adhesion of the poured silicone to the mould. The silicone material was then poured into the mould under vacuum conditions and left to cure for 72 h, after which time the skin part was extracted from the mould (Fig. 8).

The skin covering was placed on the neonatal skull phantom. The produced phantom has been evaluated by the NPL co-investigators together with clinicians, who confirmed the realistic appearance of the phantom. The produced skin covering was considered close to real human skin, in terms of colour and tactile response.

3.1.5. Validation

Preliminary validation of the phantom was completed with comparison with theoretical predictions (like the ones in Fig. 3), to check that the design had given the expected behaviour. Measurements were acquired scanning the phantom with a HP77020A scanner and a HP21200B phased array probe working at 2.5 MHz, which was already available at the NPL.

For the tests presented in this work, in addition to the thermocouple under the skin (position 1 in Fig. 3), a gradient thermocouple was inserted in the brain from a small hole opposite to the fontanel and maintained perpendicular to it. The gradient thermocouple (Omega) had a diameter of 1 mm and three sensors within it at a mutual distance of 3 mm, allowing measurements respectively at 2.5 mm, 5.5 mm and 8.5 mm from the transducer.

Fig. 9 shows the comparison between the theoretical results and the ones measured with the thermocouples, normalised by the theoretical value under the skin. The trend is correct in the region dominated by thermal diffusion, proving that the phantom matches the expectations. The temperature measured just under the skin, instead, is higher than the one expected. This difference is significant and should probably be attributed to the transducer model. The efficiency and properties of the transducers were in fact unknown: for a fixed output power (50 mW) the simulation assumed a piston-like motion, a typical efficiency of 29% and a specific heat capacity of 1000 J kg^{-1} K^{-1} for the results in Fig. 3. The amount of self-heating in the transducer is therefore rather

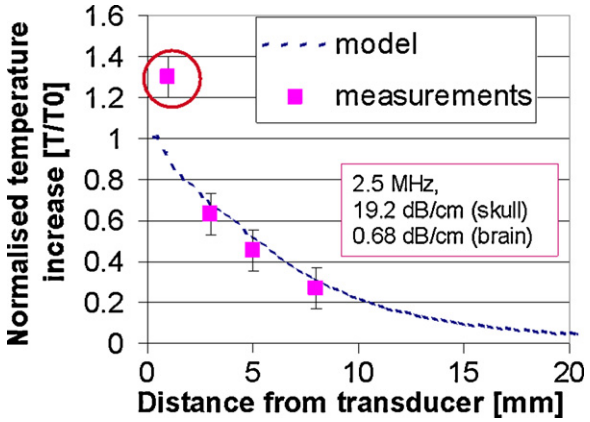

Fig. 9. Comparison between the measurements and the modelling. Values were normalised to the theoretical value read by the thermocouple in position 1 of figure.

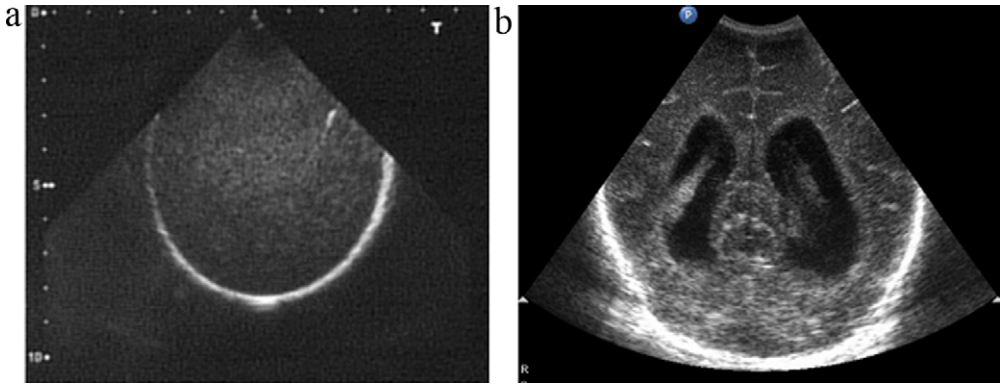

Fig. 10. Appearance of the skull-like phantom as seen using ultrasound (a). Also shown here is the appearance of a real neonatal head during a typical scan, for comparison (b).

uncertain in the model. This behaviour, which might have a clinical relevance, will be discussed in detail elsewhere.

A second, more important validation of the phantom came from the feedback received from the clinicians. The skull mimic was considered to be a good representation of neonatal head in terms of its attenuation and the nature of the speckle seen in the image. The normal preset settings gave good images, which were qualitatively similar to those of a neonatal head (see Fig. 10). The internal shape was judged to be good, with shell appearing as a bright line in the ultrasound image in the same general position and with the same general shape as the skull.

The silicone skin mimic was judged to be a bit stiff compared to scalp, and the fontanel was excessively depressed, especially when larger transducer were used. Most users, however, were impressed by the similarities and found the overall experience to be quite realistic. Several users commented that this would be a useful training tool, since all practical neonatal head training was carried out using neonates. There are many practical and ergonomic aspects of scanning which could be practised in advance with a good phantom. It was told that no phantoms of this type were available. The authors were also advised that introducing internal structure into the brain mimic, would make the scanning process even more realistic. This lead to a further modification of the brain material to produce internal structures, which will be discussed in another work.

4. Discussion

For the bone mimic, the attenuation coefficient of the material was defined as the target property to be replicated into the 3DP simulation material. Three different infiltrants were tested: epoxy resin, polyester resin and paraffin wax. An attenuation coefficient of 6.8 dB cm^{-1} at 1 MHz was measured in the epoxy infiltrated samples, which was considered in the range of neonatal skull bone by the co-investigators of NPL. In the work of Truscott et al. [17] epoxy material (Araldite^{TM} CW 1302 epoxy + Araldite^{TM} HY 1300 hardener) was tested for simulating the attenuation coefficient of bone tissue. They measured an attenuation coefficient of approximately 3.7–3.8 dB cm^{-1} (at 1 MHz), less than that recorded by the in the present study. This could be due to the characteristics of the composite material, which comprises of the 3DP powder/binder material and the epoxy resin. Several factors, such as the reflection losses at the epoxy-powder interfaces, might have determined a higher attenuation coefficient than epoxy resin alone. The attenuation coefficient of polyester resin-infiltrated samples was of 64.9 dB cm^{-1} (at 1 MHz), which could be possibly due to the specific transmission properties and physical properties of the polyester resin.

Fine-wire thermocouples (FWTCs) were more suited to this specific embedding procedure than TC thermocouples. The in-process monitoring method [23] found a further application in the monitoring of the embedding process of the thermocouples. The acquired images allowed the ascertainment of the correct positioning of the thermocouple probe, which has to be located within a specific area, of 2 mm in diameter. The results indicated some variability in the position of the thermocouple, which had to be expected, due to the methodology followed for the initial placement. However, the achieved accuracy fulfilled the requirements and the TC probe was within the target area. Factors affecting the location of the thermocouple may include the manual positioning of the thermocouple in the powder bed and the action of the roller spreading the powder. This issue can be reduced by aligning the FWTC along the roller's movement axis.

The adoption of a DRT technique using SLA technology resulted in the time-efficient and precise manufacture of the mould for the skin covering. Compared with other RP processes, SLA allowed a better surface finish of the mould, with little post-processing required. The low viscosity of the RTV2403 silicone permitted an acceptable flow within the cavity of the mould, which was of approximately 1.5 mm in thickness. The casting under vacuum condition was essential to ensure the success of the process, and avoid the presence of air bubbles within the casted part. A series of the same skin mouldings were obtained and tested on the skull phantom for fitting control. The produced skin covering was considered very realistic by the clinicians.

5. Conclusions

A realistic neonatal skull phantom for ultrasound testing has been proposed. This phantom could be further developed to become both a training tool and a method to objectively assess the thermal effect of ultrasound examination and determine the appropriateness of current scanning protocols.

The findings confirm the capability of 3DP process in reproducing the acoustic properties of neonatal skull bone with appropriate post-processing methods (i.e. infiltration). The use of an AM approach will allow the manufacture of more geometrically complex ultrasound phantoms, which could be obtained for example from reverse engineering of tomographic dataset of living patients.

The in-process embedding of a fine-wire thermocouple (FWTC) into the 3DP phantom represents a novel application of in the field of AM, which could be extended to other components or prototyping processes. The location of the FWTC allows the effective monitoring of the temperature rise in the bone-mimic material. The use of a specific machine vision system was essential for the correct positioning of the thermocouple during the embedding procedure.

Acknowledgment

The authors acknowledge the funding by the UK Department of Health, through contract RRX 113.

Conflict of interest

The authors declare that they have no proprietary, financial, professional or other personal interests of any nature or kind that could be construed as influencing the position presented in the manuscript entitles "Three-Dimensional Printing (3DP) of neonatal head phantom for ultrasound: Thermocouple embedding and simulation of bone".

References

[1] Couture A, Veyrac C. Transfontanellar Doppler imaging in neonates. Berlin: Springer; 2001.
[2] Sanders RC, Winter TC. Clinical sonography: a practical guide. Philadelphia, USA: Lippincott Williams and Wilkins; 2007.
[3] Vella GY, Humphrey VF, Duck FA, Barnett SB. Ultrasound-induced heating in foetal skull bone phantom and its dependence on beam width and perfusion. Ultrasound in Medicine and Biology 2003;29(6):779–88.
[4] International Commission on Radiological Protection ICRP. Basic anatomical and physiological data for use in radiological protection: reference values. Annals of the ICRP 2002:32.
[5] Memoli G, Shaw A, Gélat P, Sadhoo N, Osborne J, Robinson H, et al. A survey on clinical practice in neonatal ultrasound: preliminary results. In: Poster presented at IPEM meeting. 2009.
[6] Bude RO, Adler RS. An easily-made, low-cost, tissue-like ultrasound phantom. Journal of Clinical Ultrasound 1995;23:271–3.
[7] Rickey DW, Picot PA, Christopher DA, Fenster A. A wall-less vessel phantom for Doppler ultrasound studies. Ultrasound in Medicine and Biology 1995;21(9):1163–76.
[8] Demitri C, Luciana M, Montagna F, Sannino A, Maffezzoli A. Acrylic-based hydrogel phantom for in-vitro ultrasound contrast agent characterization. Virtual and Physical Prototyping 2007;2(4):191–6.
[9] Langton CM, Whitehead MA, Langton DK, Langley G. Development of a cancellous bone structural model by stereolithography for ultrasound

characterisation of the calcaneus. Journal of Medical Engineering and Physics 1997;19(7):599–604.
[10] Suwanprateep J. Comparative study of 3DP material systems for moisture resistance application. Rapid Prototyping Journal 2007;13(1):48–52.
[11] Pilipovic A, Raos P, Sercer M. Experimental analysis of properties of materials for rapid prototyping. The International Journal of Advanced Manufacturing Technology 2009;40(1–2):105–15.
[12] Gatto M, Harris RA, Sama A, Watson J. Investigating the effectiveness of three-dimensional printing for producing realistic physical surgical training phantoms. In: Annals of DAAM & proceedings of the 21st international DAAM symposium. 2010. p. 1529–31.
[13] Andre' MP, Craven JD, Greenfield MA. Measurement of the velocity of ultrasound in the human femur in vivo. Medical Physics 1980;7:324–30.
[14] Tavakoli MB, Evans JA. Dependence of the velocity and attenuation of ultrasound in bone on the mineral content. Physics in Medicine and Biology 1991;36(11):1529–37.
[15] Shaw A, Pay NM, Preston RC. Assessment of the likely thermal index values for pulsed Doppler ultrasonic equipment – stages II and III: experimental assessment of scanner/transducer combinations. NPL report CMAM 12; March 1998.
[16] Shaw A, Pay NM, Preston RC, Bond AD. Proposed standard thermal test object for medical ultrasound. Ultrasound in Medicine & Biology 1999;25(1):121–32.
[17] Truscott JC, Milner R, Clarke AJ, Evans JA. Towards an ultrasonic bone phantom. In: Abstracts of the IPSM Golden Jubilee Congress. York: IPSM; 1993. p. 151.
[18] Clarke AJ, Evans JA, Truscott JG, Milner R, Smith MA. A phantom for quantitative ultrasound of trabecular bone. Physics in Medicine and Biology 1994;39:1677–87.
[19] Tatarinov A, Sarvazyan N, Sarvazyan A. Use of multiple acoustic wave modes for assessment of long bones: model study. Ultrasonics 2005;43:672–80.
[20] Culjat MO, Goldenberg D, Tewari P, Singh RS. Tissue substitutes for ultrasound imaging. Ultrasound in Medicine and Biology 2010;36(6):861–73.
[21] Child Growth Foundation. Duodecimal growth Charts; 1996. p. 1.
[22] Paladini D, Vassallo M, Sglavo G, Pastore G, Lapadula C, Nappi C. Normal and abnormal development of the fetal anterior fontanelle: a three-dimensional ultrasound study. Ultrasound in Obstetrics and Gynecology 2008;32(6):755–61.
[23] Gatto M, Harris RA. Non-destructive analysis (NDA) of external and internal structures in 3DP. Rapid Prototyping Journal 2011;17(2):128–37.
[24] International Electrotechnical Commission, IEC 60601-2-37 (ed. 2.0). Medical electrical equipment – part 2-37: particular requirements for the basic safety and essential performance of ultrasonic medical diagnostic and monitoring equipment; 2008.
[25] Hill CR. Physical principles of medical ultrasound. Weinheim: Wiley WCH; 1987.
[26] Duck FA. Physical properties of tissue. London: Academic Press; 1990.
[27] International Commission on Radiation Units and Measurements – ICRU. Report 61, Tissue substitutes, phantoms and computational modelling in medical ultrasound; 1998.
[28] Harris RA, Fouchal F, Hague RM, Dickens PM. Quantifying part irregularities and subsequent morphology manipulation in stereolithography plastic injection moulding. Plastic, Rubber and Composites 2004;33(2–3):92–8.
[29] Sachs EM, Cima MJ, Williams P, Brancazio D, Cornie J. Three-dimensional printing-rapid tooling and prototypes directly from a CAD model. Journal of Engineering for Industry 1999;114(4):481–8.